Available online at www.sciencedirect.com
SCIENCE DIRECT
Polymer 46 (2005) 8297–8305
polymer
www.elsevier.com/locate/polymer

Effect of uniaxial drawing on surface chain structure and surface tension of poly(trimethylene terephthalate) film

Young Gyu Jeong, Woo Jin Bae, Won Ho Jo*

Hyperstructured Organic Materials Research Center, School of Materials Science and Engineering, Seoul National University, Seoul 151-742, South Korea

Received 28 January 2005; received in revised form 15 June 2005; accepted 25 June 2005
Available online 27 July 2005

Abstract

Changes in the surface chain structure and the critical surface tension of poly(trimethylene terephthalate) (PTT) film under uniaxial drawing were examined by polarized attenuated total reflection infrared (ATR-IR) spectroscopy and contact angle measurement. It was observed from the stress-draw ratio curve and density measurement that the strain-induced crystallization occurs at the draw ratio of 2.5. From the ATR-IR spectra, it was also realized that the surface chain structure changes with the draw ratio, showing a remarkable increase in the surface crystallinity at the draw ratio between two and three. The critical surface tension of uniaxially drawn films increases with the draw ratio due to an increase in the surface crystallinity developed by the strain-induced crystallization. It is concluded that the surface properties of PTT film such as the chain structure at the surface and the critical surface tension are very closely related to the condition of uniaxial drawing.

Keywords: Poly(trimethylene terephthalate); Surface crystallinity; Surface tension

1. Introduction

Poly(trimethylene terephthalate) (PTT) has recently attracted much interest from both industry and academia, because of its excellent thermal and mechanical properties for fiber- and film-forming material. It is well known that the elastic recovery of PTT fiber is superior to that of poly(ethylene terephthalate) (PET) and poly(butylene terephthalate) (PBT) [1,2], since the conformation of trimethylene unit in the crystal structure is coiled (*gauche/gauche*) [3,4], unlike the ethylene unit (*trans*) of PET [5,6] and the butylene unit (*gauche/trans/gauche*) of PBT [7–10]. Although bulk properties such as crystallization and mechanical properties of PTT have been studied extensively because the tensile deformation and crystallization are critical phenomena in fiber and film-forming processes [11–23], fundamental understanding of surface properties of PTT has been so limited. Therefore, studies on surface properties of PTT, especially in relation to the deformation and crystallization, need to be pursued.

The attenuated total reflection infrared (ATR-IR) spectroscopy has been widely used to characterize the surface chain structure of polymeric materials, since the IR absorption occurs mainly at the surface [12,24–31]. The penetration depth of IR beam, which gives an approximate sampling depth into the polymer, is usually in the range of less than a few microns, depending on the refractive index of the ATR crystal, the angle of incidence, and the wavelength of interest. Another important aspect of the ATR-IR spectroscopy is that the electric field of the evanescent wave at the surface exists in all three spatial directions. Therefore, changes in the surface structure by deformation and crystallization can be investigated quantitatively along three principal directions [12,25–27,30,31].

The contact angle measurement is one of the most sensitive methods that provide information on the surface properties which are governed solely by the outermost polymer surface of a few angstroms in thickness [32]. Thus, it is possible to gain a deep insight into the characteristic surface properties of polymers such as surface tension, heterogeneity, roughness, hydrophilicity–hydorphobicity balance, reorientation of surface groups, etc. [33–40].

* Corresponding author. Tel.: +82 2 880 7192; fax: +82 2 885 1748.
E-mail address: whjpoly@plaza.snu.ac.kr (W.H. Jo).

0032-3861/$ - see front matter © 2005 Elsevier Ltd. All rights reserved.
doi:10.1016/j.polymer.2005.06.071

In the present study, we investigate primarily the change of surface properties such as surface chain structure and surface tension of PTT film under uniaxial deformation and crystallization using the polarized ATR-IR spectroscopy and the contact angle measurement.

2. Experimental

2.1. Sample preparation and characterization

PTT pellets with $M_n = 17{,}000\ g\ mol^{-1}$ and $M_w = 35{,}000\ g\ mol^{-1}$ were used as received from Shell Chemical Company. The melt-quenched PTT films were prepared by compression molding into 0.2 mm thickness between hot plates at 245 °C, quenching into cooling water, and drying under high vacuum for several days. Then, the melt-quenched PTT films with the gauge length of 3 cm were drawn uniaxially at 60 °C at the strain rate of 5 cm min^{-1} using a universal tensile machine (LR 10K, Lloyd Inc.) equipped with a temperature-controlling chamber. After reaching the predetermined draw ratio, the drawn films were cooled down to 25 °C, holding their final length. In this study, uniaxially drawn PTT films with different draw ratios of 2, 3, and 4 were prepared and denoted as PTT (DR = 2), PTT (DR = 3), and PTT (DR = 4), respectively. Only the center part of uniaxially drawn films was used for analysis. Cold-crystallized film was prepared by annealing the melt-quenched film at 120 °C for 6 h. For comparison, the melt-quenched amorphous PET film was also prepared. All the films were desiccated before ATR-IR experiment and contact angle measurement.

The density, ρ_{sample}, of the film samples was calculated using the equation of $\rho_{sample} = A\rho_0/(A-B)$, where A and B denote the weight of sample measured in air and in distilled water, respectively, and ρ_0 the density of distilled water. Weights of sample in air and in distilled water were measured using a Mettler AT200 balance (Mettler-Toledo Inc.).

2.2. Polarized ATR-IR spectroscopy

In order to investigate changes in three-dimensional surface structure by uniaxial drawing, polarized ATR-IR spectra of the melt-quenched, uniaxially drawn, and cold-crystallized films were obtained using a Perkin–Elmer 2000 FT-IR spectrometer with ATR and polarizer accessories. KRS-5 was used for ATR crystal. Fig. 1 shows geometry of ATR crystal/PTT film while the Cartesian coordinate system (x, y, z) is used for analysis of three-dimensional surface structure of PTT films. Here, x-, y-, and z-axes indicate the machine direction (drawing direction), the transverse direction, and the normal direction to the film surface, respectively. By rotating the polarizer located between IR source and ATR crystal by 90°, the polarization of incident IR beam was controlled to be the transverse electric (TE) or the transverse magnetic (TM) wave. The TE and TM waves at the surface are have different effective penetration depths (d_e/λ_1) as given by [28]

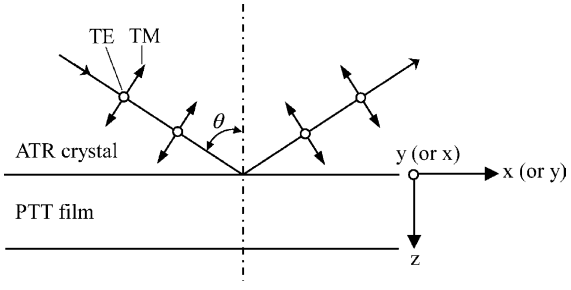

Fig. 1. ATR crystal/film geometry and orthogonal coordinate system for the polarized ATR-IR experiment.

$$\frac{d_e(\mathrm{TE})}{\lambda_1} = \frac{n\cos\theta}{\pi(1-n^2)(\sin^2\theta - n^2)^{1/2}} \tag{1a}$$

$$\frac{d_e(\mathrm{TM})}{\lambda_1} = \frac{n\cos\theta(2\sin^2\theta - n^2)}{\pi(1-n^2)[(1+n^2)\sin^2\theta - n^2](\sin^2\theta - n^2)^{1/2}} \tag{1b}$$

where $n = n_{polymer}/n_{crystal}$, $\lambda_1 = \lambda/n_{crystal}$, and θ is the incidence angle. $n_{polymer}$ and $n_{crystal}$ denote the refractive indexes of polymer and ATR crystal, respectively. In this study, $n_{polymer}$ is 1.58 for the isotropic PTT film [12], and $n_{crystal}$ is 2.38 for KRS-5 crystal. The incidence angels of 45 and 50.5° were chosen for TE and TM wave, respectively, to characterize the surface structure at the same effective penetration depth. Under this condition, the effective penetration depth at 1500 cm^{-1} is about 3 μm. Four ATR spectra (TEx, TMx, TEy, and TMy) for a given film were collected by combination of the sample orientation and the polarized incident beam (TE or TM wave), as shown in Fig. 1. Each spectrum was obtained by averaging 128 scans with a resolution of 2 cm^{-1}. Since it is well recognized that the surface structure depends on the degree of ATR crystal/sample contact, all the films were clamped in the ATR accessory under a constant pressure for reproducibility. Furthermore, in order to eliminate the difference in optical contact between samples, all the absorbances of A_{TEx}, A_{TMx}, A_{TEy}, and A_{TMy} were normalized with the reference band at 1408 cm^{-1} (C–C stretching of the phenylene ring in PTT), whose intensity was found to be unchanged regardless of deformation or crystallization [12,14,41]. From four absorbances (A_{TEx}, A_{TMx}, A_{TEy}, and A_{TMy}) obtained experimentally, spatial absorbances (A_x, A_y, and A_z) along three principal directions were calculated using the following relations [27]:

$$A_{TEx} = \alpha A_x \tag{2a}$$

$$A_{TMx} = \beta A_y + \gamma A_z \tag{2b}$$

$$A_{TEy} = \alpha A_y \tag{2c}$$

$$A_{TMy} = \beta A_x + \gamma A_z \quad (2d)$$

where α, β, and γ, which are functions of the refractive index of sample ($n_{polymer}$), incidence angle (θ), and refractive index of ATR crystal ($n_{crystal}$), were calculated to be 9.15, 1.94, and 16.37 for the TE wave and 5.10, 1.89, and 7.28 for the TM wave, respectively [24]. For quantitative analysis of ATR-IR spectra, the overlapped bands were deconvoluted by curve fitting where the linear baseline correction was made. All bands were fitted as a mixture of Gaussian and Lorentzian function. The band position, bandwidth, and intensity were allowed to vary during iteration.

2.3. Contact angle and surface roughness measurements

The sessile drop method was used for measuring the static contact angles (θ) of various liquids on the films [32]. The contact angle measurements were carried out at 25 °C using various contact liquids with a wide range of liquid–vapor surface tensions (γ_{LV}), as listed in Table 1. The contact angle was determined by averaging five measurements. The critical surface tension (γ_c) was evaluated using the method proposed by Zisman [33–35].

In order to investigate the effect of surface roughness on contact angle, the surface roughness (R_a and R_q) of film was measured using an atomic force microscopy (Dimension TM300, Digital Instruments) in the tapping mode. The average roughness, R_a, is the average deviation of the peaks and valleys from the mean elevation, and the root-mean square roughness, R_q, is the root-mean-square deviation from the mean elevation. The surface roughness was evaluated from the film area of 15×15 μm^2.

3. Results and discussion

3.1. Uniaxial deformation and crystallization

Fig. 2 shows a typical stress-draw ratio curve for the melt-quenched PTT film at 60 °C. The curve can be separated into three regions: Initial, plateau, and final regions. With increasing the draw ratio, the stress increases linearly in the initial region, remains almost constant in the plateau region, and increases again at the draw ratio of 2.5 due to the full stretching of chains between entanglement

Table 1
Contact liquids and their liquid–vapor surface tensions (γ_{LV})

Contact liquids	γ_{LV} (mN m^{-1})
α-Bromo naphthalene	44.6
Methylene iodide	50.8
Formamide	58.2
Glycerol	63.4
Distilled water	72.8

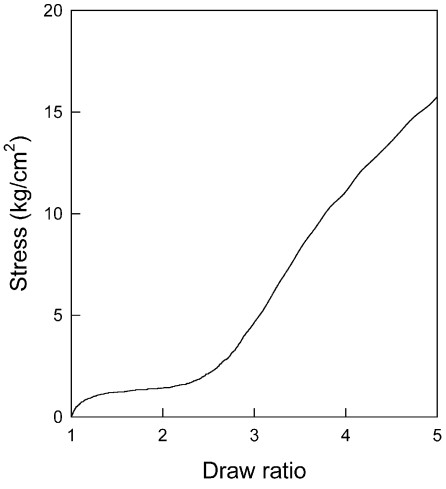

Fig. 2. A typical stress-draw ratio curve of melt-quenched amorphous PTT film during uniaxial drawing at 60 °C.

points. This stress-draw ratio behaviour is quite consistent with the results reported previously [12,14].

The densities of the melt-quenched, PTT (DR = 2), PTT (DR = 3), PTT (DR = 4), and cold-crystallized films were calculated to be 1.307, 1.311, 1.332, 1.339, and 1.368 g cm^{-3}, respectively. The density of the melt-quenched PTT film was consistent with the literature value of the purely amorphous one, 1.305 g cm^{-3} [12], which supports the accuracy of our method. Assuming a crystalline/amorphous two-phase model, the apparent crystallinity, x_c, of sample was calculated by

$$x_c(\%) = \frac{\rho_{cr}(\rho_{sample} - \rho_{am})}{\rho_{sample}(\rho_{cr} - \rho_{am})} \times 100 \quad (3)$$

where ρ_{cr} and ρ_{am} are the density of 100% crystalline sample and of totally amorphous sample, respectively. Using $\rho_{cr} = 1.427$ g cm^{-3} [4] and $\rho_{am} = 1.307$ g cm^{-3}, the bulk crystallinity of PTT (DR = 2), PTT (DR = 3), (PTT = 4), and the cold-crystallized film was calculated to be 4, 22, 28, and 53%, respectively. This result indicates that the bulk crystallinity increases considerably at the draw ratio between two and three due to the stain-induced crystallization, which is closely related with the stress-draw ratio behavior shown in Fig. 2.

3.2. Effect of uniaxial drawing on surface chain structure

Fig. 3(A)–(C) shows changes of the spatial absorbances of A_x, A_y, and A_z with the draw ratio. For the spatial absorbance of A_x, the intensities of amorphous bands at 817, 976, 1015, and 1328 cm^{-1} and crystalline bands at 932, 1358, and 1505 cm^{-1} increase with increasing the draw ratio, while the intensities of amorphous band at 1173 cm^{-1} and crystalline bands at 948 and 1463 cm^{-1} decrease, as can be seen in Fig. 3(A). The intensities of the crystalline and amorphous bands change noticeably around the draw ratio between two and three at which the strain-induced

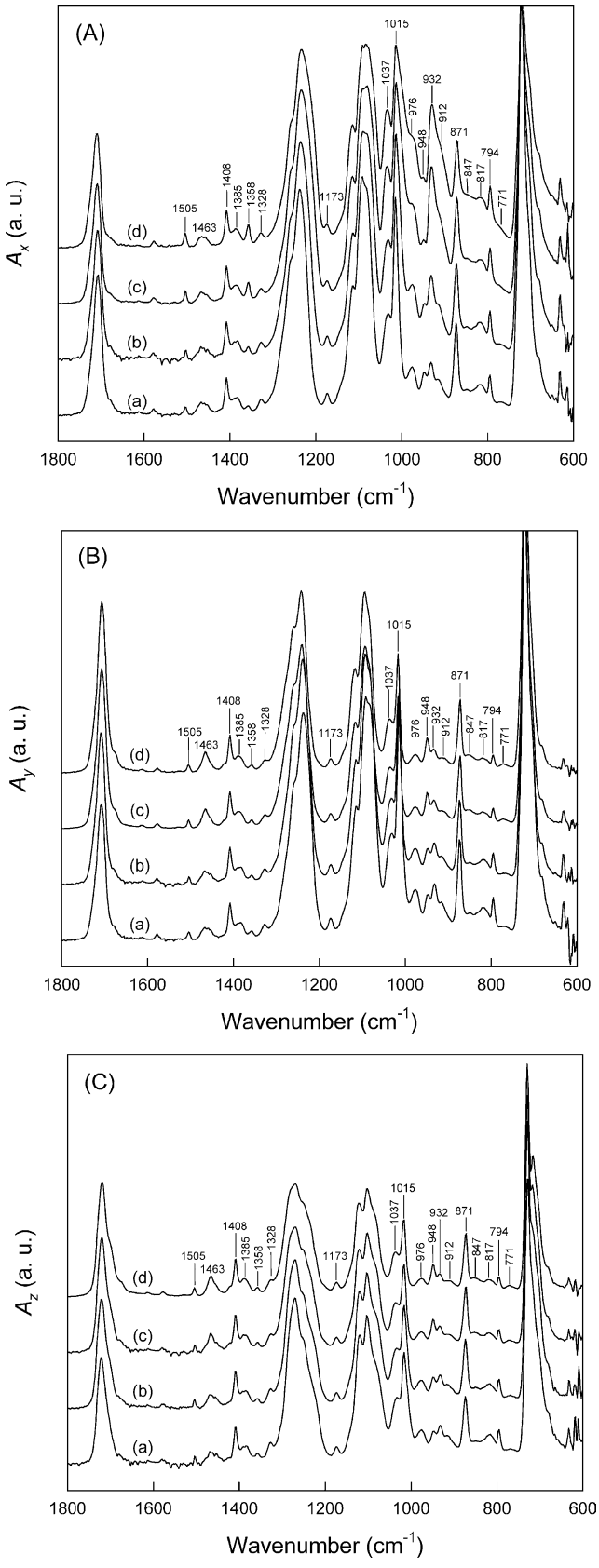

Fig. 3. Spatial absorbance spectra of (A) A_x, (B) A_y, and (C) A_z for the PTT films with different draw ratios: (a) PTT (melt-quenched); (b) PTT (DR = 2); (c) PTT (DR = 3); (d) PTT (DR = 4).

crystallization occurs. These crystalline and amorphous absorption bands have been successfully assigned and used to characterize quantitatively the crystallization as well as the orientation of PTT [12,14,42–44]. For the spatial absorbances of A_y and A_z, changes of intensities of the crystalline and amorphous bands with the draw ratio are opposite to the trend in the case of A_x, as shown in Fig. 3(B) and (C). Since x is the draw direction, it is expected that A_x is greater than A_y (or A_z) for parallel bands and A_y (or A_z) is greater than A_x for perpendicular bands. We have found that the analysis on the chain orientation of PTT by uniaxial drawing in this study was consistent with the results from previous studies [12,14,41]. Here, it is noteworthy to mention that, for the melt-quenched amorphous PTT film, the spatial absorbance of A_z is not identical with that of A_x or A_y. Considering that melt-quenched film is purely amorphous, it is expected that the difference in spatial absorbances between A_x (or A_y) and A_z originate from anisotropic conformational distribution at the surface. In other words, the chain conformational distribution in the perpendicular direction (z-axis) is different from the distribution in the direction (x- or y-axis) parallel to the film surface.

The structural factor (A_0), the average value of three spatial absorbances, is defined as [45]

$$A_0 = \frac{1}{3}(A_x + A_y + A_z) \tag{4}$$

Since the structural factor is independent of sample orientation and is proportional to the total concentration of a functional group corresponding to the specific infrared band, it provides information on the overall change in the surface structure that occur during deformation or crystallization. The structural spectra of the melt-quenched, uniaxially drawn, and cold-crystallized PTT films are shown in Fig. 4. By comparing the structural factor of the melt-quenched film with that of cold-crystallized film, it is realized that the bands at 932, 1358, 1463, and 1505 cm^{-1} correspond to crystalline phase and that the bands at 817, 976, 1015, 1173, and 1328 cm^{-1} correspond to amorphous phase [44]. For uniaxially drawn films, the intensities of crystalline bands increase with increasing the draw ratio, whereas those of amorphous bands decrease, showing a noticeable change at the draw ratio between two and three, as shown in Fig. 5.

Fig. 6 shows the structural factors associated with C=O stretching bands of the melt-quenched, uniaxially drawn, and cold-crystallized PTT films. For the melt-quenched amorphous films, the C=O stretching bands are deconvoluted with three bands of 1724, 1708, and 1678 cm^{-1}, as can be seen in Fig. 6(A). Reminding that the melt-quenched film is purely amorphous, three C=O stretching bands originate from three different conformational environments of PTT chains. On the other hand, for the cold-crystallized film, the C=O stretching bands are separated into four bands of 1724, 1708, 1696, and 1673 cm^{-1}. When the C=O

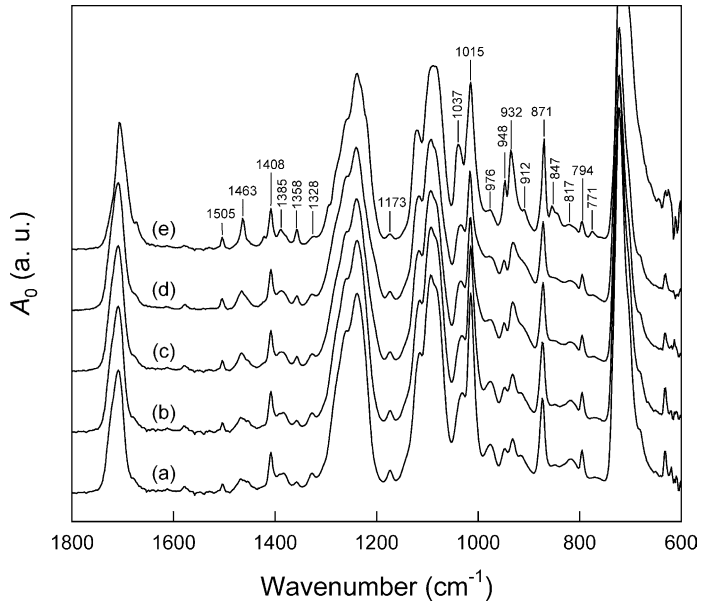

Fig. 4. The absorbance spectra of the PTT films based on structural factor: (a) PTT (melt-quenched); (b) PTT (DR = 2); (c) PTT (DR = 3); (d) PTT (DR = 4); (e) PTT (cold-crystallized).

stretching bands of amorphous film (Fig. 6(A)) are compared with those of cold-crystallized films (Fig. 6(E)), it is found that the integrated absorbances of 1724 and 1708 cm^{-1} decrease considerably due to crystallization whereas the 1678 cm^{-1} band of the amorphous film shifts to lower wavenumber of 1673 cm^{-1} and a new band develops at 1696 cm^{-1}. Therefore, it is reasonable to conclude that the absorbances at 1724, 1708, and 1678 cm^{-1} correspond to the C=O stretching bands in amorphous state, while those of 1673 and 1696 cm^{-1} correspond to the C=O stretching bands in crystalline state. For the uniaxially drawn films, the intensity of crystalline C=O stretching band at 1696 cm^{-1} increases noticeably at the draw ratio between two and three at which the strain-induced crystallization occurs.

Since the trimethylene groups of PTT backbone in the crystal structure take *gauche*/*gauche* conformation, it is clear that the *gauche* content increases with the degree of crystallinity. Since the 932 and 817 cm^{-1} bands originate from *gauche* conformer and *trans* conformer of trimethylene units, respectively [14], with increasing the draw ratio the intensity of the 932 cm^{-1} band increases, whereas the intensity of 817 cm^{-1} band decreases, as shown in Fig. 5. Here, it is noted that larger draw ratio gives higher crystallinity. Chuah [14] has recently evaluated the *gauche* content of uniaxially drawn PTT films using the intensity ratio of 932 to 817 cm^{-1} band, assuming a crystalline/amorphous model. Similarly, the *gauche* content of the uniaxially drawn films prepared in this study is estimated by

$$\textit{gauche}\ \text{content}\ (\%) = \frac{I_{932}}{I_{932} + 1.23 I_{817}} \times 100 \qquad (5)$$

where I_{932} and I_{817} are intensities of 932 and 817 cm^{-1} bands, respectively. The constant of 1.23 means that I_{932} is

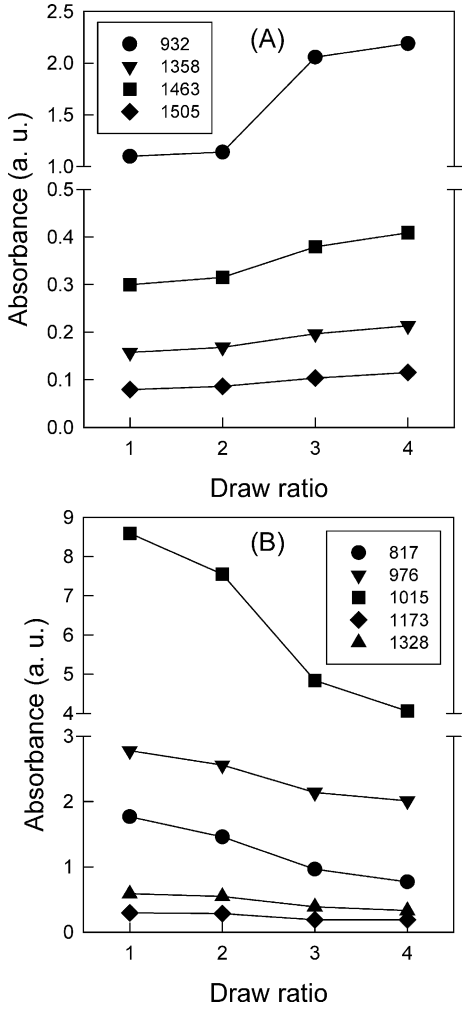

Fig. 5. Changes of intensities of (A) crystalline and (B) amorphous bands as a function of the draw ratio.

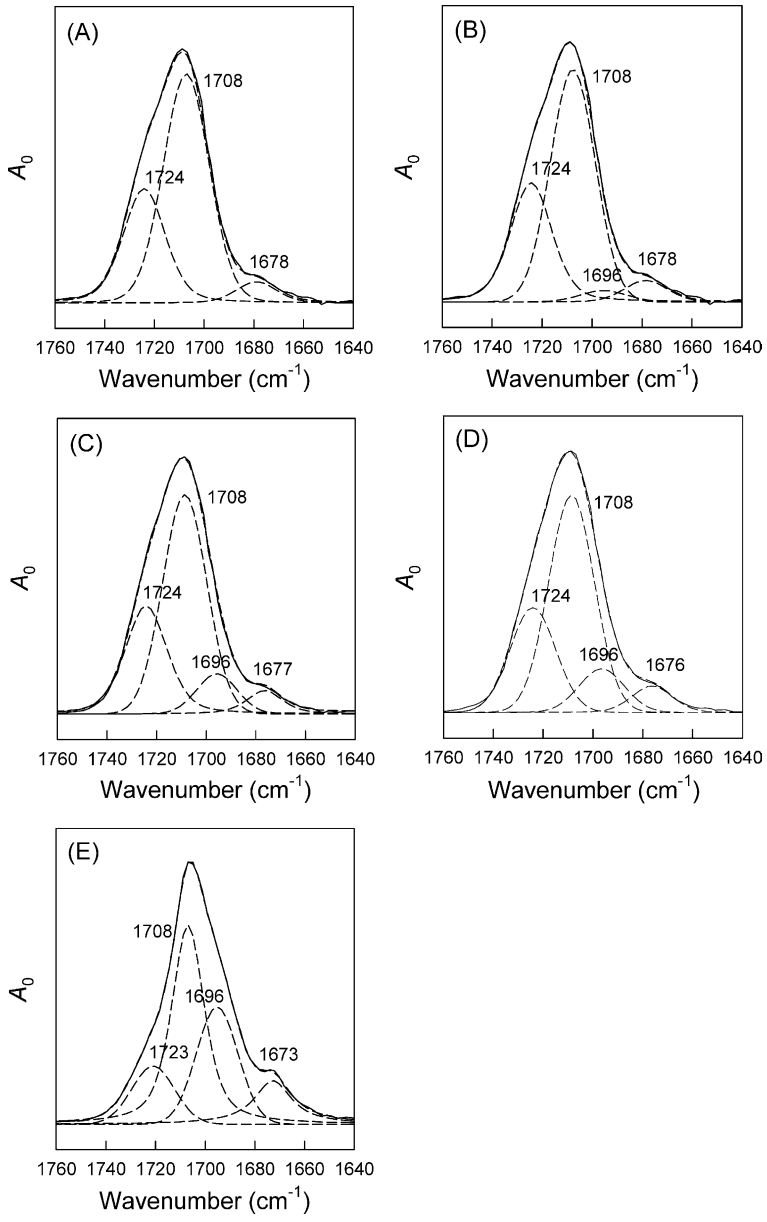

Fig. 6. The structural factors associated with C=O stretching bands: (A) PTT (melt-quenched); (B) PTT (DR=2); (C) PTT (DR=3); (D) PTT (DR=4); (E) PTT (cold-crystallized). The solid lines are the experimental data and the dotted lines are the deconvoluted bands.

1.23 times stronger than I_{817} for drawn films. The *gauche* contents of the melt-quenched film, PTT (DR=2), PTT (DR=3), and PTT (DR=4) are calculated to be 33.4, 38.7, 63.4, and 69.7%, respectively. Since the melt-quenched film is fully amorphous, it is reasonable to assume that the amorphous phase of PPT has the *gauche* content of 33.4% in trimethylene unit. Considering that the *gauche* conformation of trimethylene unit in the amorphous phase transforms to the *trans* conformation by uniaxial drawing, it is obvious that the increase in the *gauche* content of uniaxially drawn films results from the surface crystallinity developed by strain-induced crystallization. The surface crystallinity of uniaxially drawn films increases considerably around the draw ratio two and three at which the strain-induced crystallization starts to occur. The *gauche* content of cold-crystallized film was estimated to be 84.0% using Eq. (5), although the constant 1.23 in Eq. (5) is only valid for uniaxially drawn films. In short, it is concluded that the surface chain structure such as the chain conformation and the crystallinity at the surface is changed considerably by uniaxial drawing.

3.3. Effects of deformation and crystallization on critical surface tension

In order to measure the critical surface tension (γ_c) of films, the contact angles (θ) of contacting liquids on film were measured and their cosine values are plotted as a

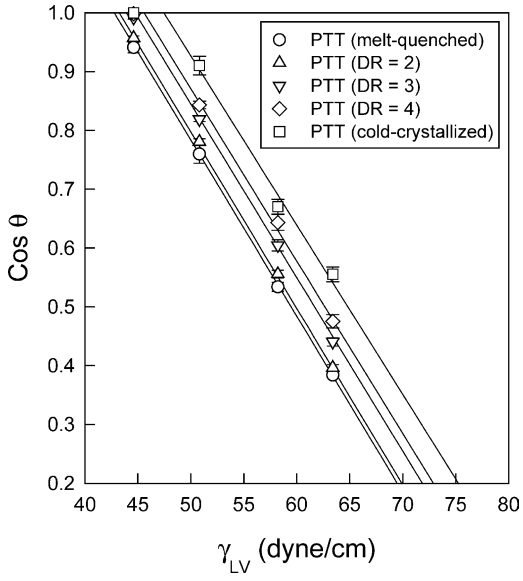

Fig. 7. Zisman plots for estimating the critical surface tensions of the melt-quenched, uniaxially drawn, and cold-crystallized PTT films.

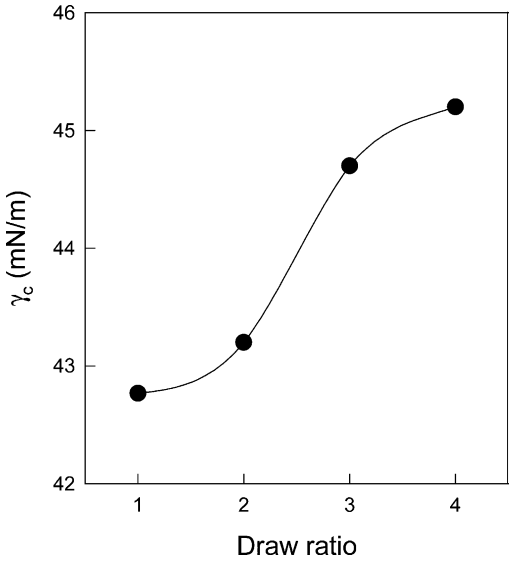

Fig. 8. A plot of the critical surface tension of uniaxially drawn PTT films against the draw ratio.

function of liquid–vapor surface tensions (γ_{LV}) of contacting liquids, as shown in Fig. 7. The critical surface tension is estimated by extrapolating linearly the plot of cos θ versus γ_{LV} to cos $\theta = 1$, where the contact angle of water ($\gamma_{LV} = 72.8$ mN m^{-1}) is excluded from the linear regression because of its large deviation from linearity. Indeed, it is generally known that hydrogen-bonding liquids usually deviate from linearity [32,46]. The critical surface tensions estimated by the above method are listed in Table 2. It was found that the critical surface tension (44.3 mN m^{-1}) of the amorphous PET film in this study is quite consistent with the values obtained by the Zisman method (43 mN m^{-1}) [47] and the equation of state method (44.0 mN m^{-1}) [32]. This supports that the contact angle data and critical surface tensions measured in this study are reliable.

It was also noted that the critical surface tension of the melt-quenched PTT film is slightly lower than that of PET, as can be seen in Table 2. The surface tension of amorphous polymer (γ^{am}) can be estimated by the expression [48,49]:

$$\gamma^{am} = \left(\frac{P}{V_a}\right)^4 \quad (6)$$

where P is the parachor of repeat unit and V_a is the molar volume of the amorphous phase. Using the group contributions to P and V_a [50], the surface tensions of amorphous PTT and PET are estimated to be 43.0 and 44.4 mN m^{-1}, respectively. These values agree well with the experimental ones (42.8 and 44.3 mN m^{-1}). For uniaxially drawn PTT films, the critical surface tension increases from 42.8 to 45.4 mN m^{-1} with increasing the draw ratio, exhibiting an abrupt change at the draw ratio between two and three, as shown in Fig. 8.

Surface properties of polymers may be influenced considerably by surface roughness and chemical heterogeneity at the surface. Busscher et al. [38] examined the effect of surface roughness, controlled by polishing and abrasion, on the wetting behavior of at least 12 different commercial polymers and concluded that the value of surface roughness less than 0.1 μm does not affect the wettability of the surface. On the other hand, Miller et al. [39] reported that even extremely low value of surface roughness with nanometer scale might affect the wetting behavior of the polytetrafluoroethylene. When the surface roughness of all the PTT and PET films are compared with each other, there is no systematically significant difference in the surface

Table 2
Critical surface tensions of PTT and PET films

Sample	γ_c (mN m^{-1})
PTT (melt-quenched)	42.8
PTT (DR = 2)	43.2
PTT (DR = 3)	44.7
PTT (DR = 4)	45.4
PTT (cold-crystallized)	47.5
PET (melt-quenched)	44.3

Table 3
Surface roughness of PTT and PET films

Sample	R_a (nm)[a]	R_q (nm)[b]
PTT (melt-quenched)	4.3	6.9
PTT (DR = 2)	7.4	14.7
PTT (DR = 3)	6.7	8.6
PTT (DR = 4)	7.9	13.8
PTT (cold-crystallized)	5.4	8.2
PET (melt-quenched)	4.5	7.5

[a] Average roughness defined as the average deviation of the peaks and valleys from the mean elevation.

[b] Root-mean-square roughness defined as the root-mean-square deviation from the mean elevation.

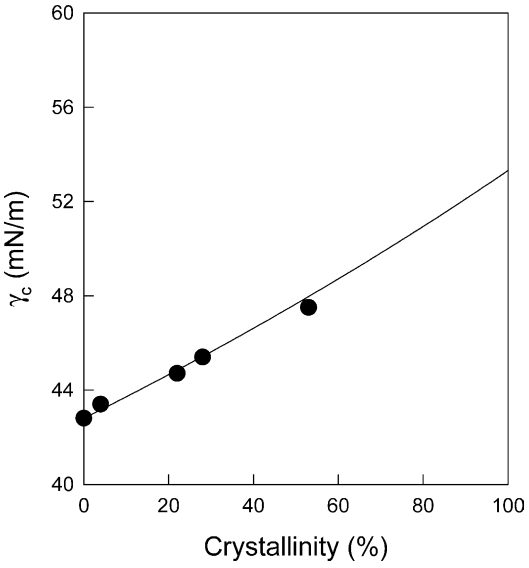

Fig. 9. A linear relation between the critical surface tension and the surface crystallinity.

roughness between samples, as can be seen in Table 3. Therefore, it is valid to assume that the affect of surface roughness on the contact angle and the critical surface tension is rather small and negligible. Reminding that the surface crystallinity of PTT films increases with increasing the draw ratio, we can conclude that the increase in the critical surface tensions of the uniaxially drawn and cold-crystallized PTT films arise from the surface crystallinity developed by strain-induced crystallization and annealing. It has been reported that the surface tension of a semicrystalline polymer is very closely related to its surface crystallinity [51,52]. When the critical surface tension of PTT films is plotted against the surface crystallinity, assuming that the surface crystallinity of PTT film is equal to the bulk crystallinity obtained by density measurement, a linear relation is observed, as shown in Fig. 9.

4. Conclusions

Changes in the surface chain structure with uniaxial deformation were characterized using polarized ATR-IR spectroscopy, and the critical surface tension was estimated by contact angle measurement. It was observed that the chain conformation as well as the degree of crystallinity at the film surface is considerably changed with the draw ratio due to the stain-induced crystallization, which occurs around the draw ratio of 2.5. Consequently, the critical surface tension of uniaxially drawn films increases with the surface crystallinity developed by the strain-induced crystallization. Similarly, the critical surface tension of the cold-crystallized film becomes larger due to the increased surface crystallinity. In short, it is concluded that uniaxial drawing accompanied with crystallization affects significantly the surface chain structure, resulting in a change of the surface tension of PTT film.

Acknowledgements

The authors thank the Korea Science and Engineering Foundation for financial support through the Hyper-structured Organic Materials Research Center.

References

[1] Jakeways R, Ward IM, Wilding MA, Hall IH, Desborough IJ, Pass M G. J Polym Sci Polym Phys 1975;13:799.
[2] Ward IM, Wilding MA, Brody H. J Polym Sci Polym Phys 1976;14:263.
[3] Poulindandurand S, Perez S, Revol JF, Brisse F. Polymer 1979;20:419.
[4] Desborough IJ, Hall IH, Neisser JZ. Polymer 1979;20:545.
[5] Daubeny RdeP, Bunn CW, Brown CJ. Proc R Soc London Ser A 1954;226:531.
[6] Fakirov S, Fischer EW, Schmidt GF. Makromol Chem, Macromol Chem Phys 1975;176:2459.
[7] Jakeways R, Smith T, Ward IM, Wilding MA. J Polym Sci Polym Lett 1976;14:41.
[8] Hall IH, Pass MG. Polymer 1976;17:807.
[9] Yokouchi M, Sakakibara Y, Chatani Y, Tadokoro H, Tanaka T, Yoda K. Macromolecules 1976;9:266.
[10] Tashiro K, Nakai Y, Kobayashi M, Tadokoro H. Macromolecules 1980;13:137.
[11] Jang SS, Jo WH. J Chem Phys 1999;110:7524.
[12] Lee HS, Park SC, Kim YH. Macromolecules 2000;33:7994.
[13] Cho JW, Woo KS. J Polym Sci Polym Phys 2001;39:1920.
[14] Chuah HH. Macromolecules 2001;34:6985.
[15] Wang BJ, Li CY, Hanzlicek J, Cheng SZD, Geil PH, Grebowicz J, et al. Polymer 2001;42:7171.
[16] Grebowicz JS, Brown H, Chuah HH, Olvera JM, Wasiak A, Sajkiewicz P, et al. Polymer 2001;42:7153.
[17] Wu J, Schultz JM, Samon JM, Pangelinan AB, Chuah HH. Polymer 2001;42:7141.
[18] Wu G, Li HW, Wu YQ, Cuculo JA. Polymer 2002;43:4915.
[19] Wu PL, Woo EM. J Polym Sci Polym Phys 2003;41:80.
[20] Chen KQ, Tang XZ. J Appl Polym Sci 2004;91:1967.
[21] Chuang WT, Hong PD, Chuah HH. Polymer 2004;45:2413.
[22] Mackintosh AR, Liggat JJ. J Appl Polym Sci 2004;92:2791.
[23] Frisk S, Ikeda RM, Chase DB, Kennedy A, Rabolt JF. Macromolecules 2004;37:6027.
[24] Flournoy PA, Schaffer WJ. Spectrochim Acta 1966;22:5.
[25] Flournoy PA. Spectrochim Acta 1966;22:15.
[26] Sung CSP. Macromolecules 1981;14:591.
[27] Hobbs JP, Sung CSP, Krishnan K, Hill S. Macromolecules 1983;16:193.
[28] Harrick NJ. Internal reflection spectroscopy. 3rd ed. Ossing: Harrick Scientific; 1987.
[29] Landreth BM, Stupp SI. Macromolecules 1987;20:2083.
[30] Kaito A, Nakayama K. Macromolecules 1992;25:4882.
[31] Lofgren EA, Jabarin SA. J Appl Polym Sci 1994;51:1251.
[32] Wu S. Polymer interface and surface. New York: Marcel Dekker; 1982.
[33] Fox HW, Zisman WA. J Colloid Sci 1950;5:514.
[34] Fox HW, Zisman WA. J Colloid Sci 1952;7:109.
[35] Fox HW, Zisman WA. J Colloid Sci 1952;7:428.
[36] Baier RE, Zisman WA. Macromolecules 1970;3:70.

[37] Yasuda H, Sharma AK. J Polym Sci Polym Phys 1981;19:1285.
[38] Busscher HJ, Vanpelt AWJ, Deboer P, Dejong HP, Arends J. Colloid Surf 1984;9:319.
[39] Miller JD, Veeramasuneni S, Drelich J, Yalamanchili MR, Yamauchi G. Polym Eng Sci 1996;36:1849.
[40] Tretinnikov ON, Ikada Y. Langmuir 1994;10:1606.
[41] Park SC, Liang Y, Lee HS. Macromolecules 2004;37:5607.
[42] Ward IM, Wilding MA. Polymer 1977;18:327.
[43] Bulkin BJ, Lewin M, Kim J. Macromolecules 1987;20:830.
[44] Kim KJ, Bae JH, Kim YH. Polymer 2001;42:1023.
[45] Schmidt PG. J Polym Sci 1963;1:1271.
[46] Garbassi F, Morra M, Occhiello E. Polymer surfaces from physics to technology. Chichester: Wiley; 1998.
[47] Zisman WA. Advances in chemistry series. vol. 43. Washington DC: American Chemical Society; 1964.
[48] Roe RJ. J Phys Chem 1965;69:2809.
[49] Lee IJ, Muir WM, Lyman DJ. J Phys Chem 1965;69:3220.
[50] Van Krevelen DW. Properties of polymers. 3rd ed. Amsterdam: Elsevier Scientific; 1990.
[51] Schonhorn H, Ryan FW. J Phys Chem 1966;70:3811.
[52] Schonhorn H. Macromolecules 1968;1:145.